

Article

Structural Characterization of Perpendicularly Aligned Submicrometer-Thick Synthetic Glycolipid Polycrystalline Films Using Conventional X-ray Diffraction

Shigesaburo Ogawa¹ and Isao Takahashi^{2,*}

¹ Department of Materials and Life Science, Faculty of Science and Technology, Seikei University, Musashino-Shi 180-8633, Japan; s.ogawa.chem@gmail.com

² Department of Physics, School of Science and Technology, Kwansai Gakuin University, Sanda 669-1337, Japan

* Correspondence: suikyo@kwansai.ac.jp; Tel.: +81-79-565-9722

Academic Editor: Shujun Zhang

Received: 30 October 2017; Accepted: 29 November 2017; Published: 1 December 2017

Abstract: The structural analysis of the synthetic glycolipid crystalline phase has been performed during the past few decades; however, it has not been sufficiently understood in terms of both static and dynamic aspects. We have recently shown that grazing incidence X-ray diffraction (GIXD) affords better information than conventional powder X-ray diffraction (PXRD) for the crystal structure analysis of octyl β -D-galactoside (MO β Gal) using sub-micrometer-thick crystalline films and a two-dimensional detector, together with a synchrotron radiation source. However, access to this technique is not universal because of the limited machine time at the required synchrotron radiation sources. Herein, we employed XRD analysis on MO β Gal hemihydrate crystalline films using commercial X-ray sources instead of synchrotron radiation sources to extend the availability of the methodology. We investigated some technical aspects of the methodology, such as incident angle and radiation time, using MO β Gal polycrystalline films with different thicknesses in order to obtain sufficient reciprocal data for identifying the lattice constants with conventional X-ray sources. Complementary uses of GIXD with a two-dimensional detector, with much higher incident angles than the total reflection angle using a NANO-Viewer system and out-of-plane and in-plane measurements using SmartLab, enabled us to determine the complete lattice parameters for the MO β Gal hemihydrate crystalline film.

Keywords: synthetic glycolipid; X-ray diffraction; grazing incidence X-ray diffraction; structural analysis; crystalline film

1. Introduction

Since Emil Fisher first reported on alkyl glycosides in 1893 [1], synthetic glycolipids, which are relatively simple sugar amphiphiles, have been studied for over a century. Currently, various glycoside compounds are becoming commercially available. Apart from their intrinsic interest as potentially useful compounds, simpler alkyl and acyl glycosides, which can frequently be crystallized, have been expected to serve as relevant model systems for complex structural transitions that occur in the functioning of glycolipids that are found in cell membranes. One such approach involves analyzing the structures of the synthetic glycolipid crystal phases [2–5].

The crystal is a phase of molecular assembly, and there are multiple similarities between the crystal phase and the molecular arrangement of the liquid crystalline (LC) phase, which is essential for cell membrane biological functions [4,6,7]. In addition, the molecular motions in the crystal phase

are strictly restricted when compared to the LC phase; and, therefore, a quantitative clarification of the functions and effects of sugar moieties can be understood by analyzing the crystalline phases. The three-dimensional repeating lattice of crystals arising from the regular spacing of atoms or molecules within the sample yields a diffraction pattern of distinct spots, the so-called Laue spots, in the diffraction analyses. The relative locations of these spot indicate the crystal symmetry and dimensions of the unit cell according to Braggs law. If an adequate single crystal is prepared, X-ray structural analysis provides the presence of hydrogen bonding and characterizes its strength based on the atomic coordinates of the molecular assembly. Numerous crystal structures of synthetic glycolipids have been resolved via X-ray single-crystal structure analysis. In most of the cases, the bilayer structure formation of these compounds has been identified, with some exceptions [2–10]. A two-dimensional bilayer structure has been reported even for a methyl glycoside compound [11], strongly suggesting that the formation of the bilayer structure is generally favored. Owing to the characteristics of the bilayer structure, the unit cells have one long and two short axes.

On the other hand, despite the abundant reports on synthetic glycolipid crystal studies, there are several ambiguous issues remaining in synthetic glycolipid crystalline research, as follows: (1) Static aspects: Single crystal structures of β -linked alkyl-*O*-glycosides have not yet been resolved due to the difficulty in preparing adequately sized single crystals. However, in 1981, Dorset proposed that the β -anomer of octyl β -*D*-glucoside possesses crystal packing that is distinctly different from that of the α -anomer [12]. In other words, an unknown crystal structure might exist, even in the representative synthetic glycolipid crystals known to date, including commercially available compounds. (2) Dynamic aspects: Synthetic glycolipids exhibit a solid–solid phase transition in their crystalline phase [13–18]. It has been postulated that the increase in thermal motions during the heating process weakens the hydrogen bonding interaction, which allows for the rearrangement of the molecular assembly from head-to-tail packing to head-to-head packing [7,19]. Kocehrbitov and Söderman and Ericsson et al. have shown that such transitions can be observed in a thermogram if traces of water are present [20,21]. In such cases, the melting of the hemihydrate crystal occurs as a pre-transition of the main anhydrous crystal melting. However, even in the absence of trace water, solid–solid transitions can be observed for certain compounds, and there are many ambiguities remaining for many other compounds. For instance, *n*-alkyl β -*D*-glucosides of various alkyl chain lengths exhibited solid–solid phase transitions after careful water removal treatment had been performed during sample preparation for thermal analysis [22].

In most cases, (1) and (2) seemed to be observed for the same compounds. In addition, suitable single crystals would not be available after the solid–solid transition; not all of the phase transitions follow single-crystal-to-single-crystal transitions. Therefore, to clarify the dynamic nature, including solid–solid transitions with temperature variations, powder X-ray diffraction (PXRD) is the only technique that can obtain structural analysis information. However, the structural details from PXRD are not as precise as single crystal data, unless the crystal structure is so simple that it can be solved by computer simulations. Presently, the development of a methodology that is readily applicable to non-ambient condition measurements, but with increased structural details than can be obtained using conventional PXRD, is required, in particular, to understand both the static and dynamic natures of synthetic glycolipid crystals.

The method based on grazing incidence X-ray diffraction (GIXD) with a two-dimensional detector has received increased attention for identifying crystal structures of organic semiconductor thin films [23], but less attention has been paid to applying this method to the crystal structure analysis of synthetic glycolipids. On the other hand, we have recently applied the analytical methodology to the crystalline structure analysis of hemihydrate crystals of one synthetic glycolipid, octyl β -*D*-galactoside (MO β Gal) (Figure 1) [24]. We prepared relatively thick films to avoid the confinement effect by thinning the crystal structure since the structural analysis targeted the bulk crystal of synthetic glycolipid. Because of the highly aligned behavior in the LC state of synthetic glycolipid, even at sub-micrometer thicknesses, crystallization from the aligned LC state successfully afforded the perpendicularly aligned sub-micrometric polycrystalline film. The polycrystalline film, in which each crystal was randomly

aligned in parallel, but was perpendicularly aligned to the substrate, made the reciprocal images, which afforded numerous diffraction spots even without rotating the sample. The use of aligned samples was preferred for a better description of the LC phase of synthetic glycolipid [25,26], but few studies seem to apply this structural analysis method to crystal species [12]. As a result, important crystal parameters, such as lattice constants, space group, and symmetry, were analyzed for the MO β Gal hemihydrate crystal (Figure 1b), which were difficult to obtain using PXRD analysis of a non-oriented powder sample (Figure 1c). Importantly, the crystal structure consisted of a “ribbon phase”, with a large number of formula units per unit cell (Z). The space group was assumed as $P2_12_12_1$, with lattice constants, $a = 47.9\text{ \AA}$, $b = 27.4\text{ \AA}$, and $c = 4.73\text{ \AA}$, which did not obey the general tendency of $a \approx \text{bilayer length} \gg b > c \approx \text{interval of alkyl chain packing}$ that is observed for typical synthetic glycolipid crystals that are solved by single-crystal structure analysis [2–10]. Moreover, not only is the methodology useful for depicting such static crystalline structure analysis, but it is also useful for pursuing the dynamic nature of solid–solid transitions, such as dehydration and continuous structural changes in the anhydrous crystal forms as the temperature varies [24]. Solid–solid phase transitions occurred after the perpendicular alignment of polycrystalline MO β Gal crystals persisted, affording detailed structural analysis using the same sample under non-ambient atmosphere conditions. Thus, this analytical method was assumed to greatly contribute to the development of crystalline glycolipid research, which seemed to still include many unsolved issues, as mentioned above.

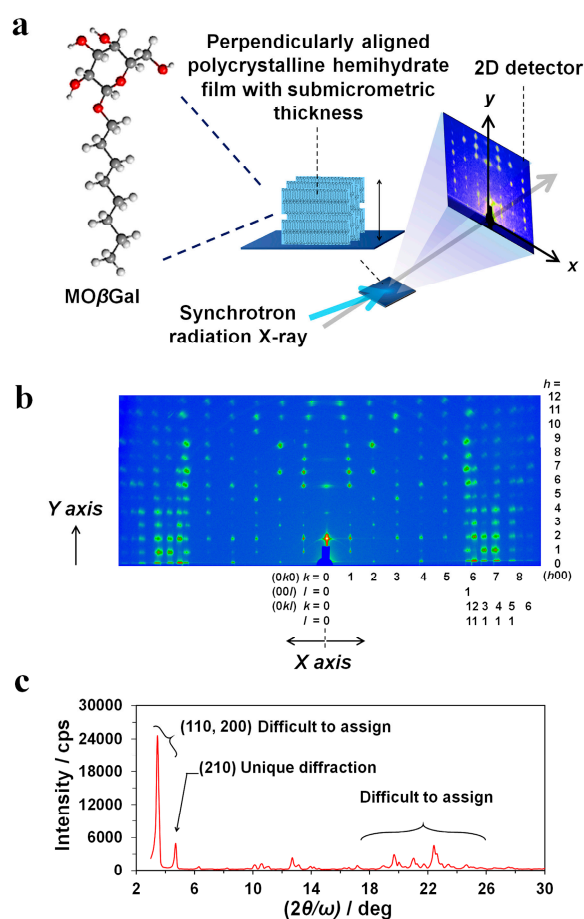


Figure 1. (a) Schematic of two-dimensional grazing incidence X-ray diffraction (GIXD) analysis for approximately 200-nm-thick octyl β -D-galactoside (MO β Gal) hemihydrate perpendicularly aligned polycrystalline films with synchrotron radiation. (b) GIXD image with the assignment of (hkl) indexes obtained for the sample shown in (a) with an incident angle of 0.17° and synchrotron radiation for 3 s at BLXU03, SPring8. (c) Powder X-ray diffraction (PXRD) image of the MO β Gal hemihydrate powder sample obtained using a conventional X-ray source (SmartLab) employing a one-dimensional detector.

However, in our previous study, the method had been based on a synchrotron X-ray system, and the experiment was performed by using a beamline at the BL03XU frontier soft-material beamline (FSBL), SPring-8, Hyogo, Japan [24]. The details of the beamline can be found in these selected review papers [27,28]. In order to obtain machine time at such institutes, a research proposal must be written and accepted, and such situations would limit the methodology to a smaller number of researchers. When considering the high usability of laboratory-scaled commercial X-ray apparatuses, it would be a significant advance if clear reciprocal images of synthetic glycolipid crystals could be obtained without synchrotron radiation X-ray systems. This idea made us consider applying the methodology based on the use of perpendicularly aligned polycrystalline films of sub-micrometer thicknesses, a two-dimensional detector, and commercially available X-ray systems to crystal structure analysis of synthetic glycolipids.

In this paper, we report on the structural analysis of the MO β Gal hemihydrate crystal using commercially available X-ray apparatuses: the NANO-Viewer (Rigaku Corp., Tokyo, Japan), equipped with a two-dimensional detector, Pilatus 100K (Rigaku Corp., Tokyo, Japan); and SmartLab (Rigaku Corp.) equipped with a scintillation detector. Here, the Pilatus 100 K detected possessed active areas of limited sizes, and therefore, the measurable XD angle range was limited. In addition, the beam size was much larger than that of a synchrotron. As a result, when compared to the synchrotron-sourced X-ray beam (Figure 1b), the resolution of the structural analysis decreased. We have investigated the diffraction conditions of the NANO-Viewer (Rigaku Corp.), such as incident angles, radiation time, and thickness of film, and we also complementarily used out-of-plane and in-plane measurements with the SmartLab system (Rigaku Corp.) in order to obtain sufficiently good reciprocal images of MO β Gal hemihydrate crystals to determine the lattice parameters of the unique crystals with laboratory scale X-ray equipment.

2. Results and Discussion

2.1. MO β Gal Polycrystalline Films with Different Thicknesses

MO β Gal polycrystalline films of various thicknesses ranging from approximately 75, 170, 640, 1300, and 3200 nm, were prepared by spin-coating aqueous MO β Gal solutions at concentrations of 5 wt%, 10 wt%, 20 wt%, 30 wt%, and 40 wt%, respectively. Film thickness in nm were determined by $77,790 \times |\text{Max Abs.}|$ around 2850 cm^{-1} , according to our previous report [24]. The as-prepared MO β Gal films readily crystallized as hemihydrate crystalline in a sealed container from the semi-humidified state. Thicker films tended to crystallize faster. Figure 2 shows the AFM images of MO β Gal films after the crystallization of the hemihydrate crystals. A scratched image of the 3200 nm thick MO β Gal film is shown; using the scratched data, the validity of this film thickness determination method was confirmed by measuring the height from the Si substrate.

As shown in Figure 2, as the film thickness increased, the surface roughness apparently increased, especially for films that were thicker than approximately 640 nm. As shown in the figure, all of the surface regions consisted of polycrystalline species with sub-micrometric to micrometric scale lengths. In previous studies, the MO β Gal tended to form fiber structures, not only in aqueous solutions, but also on solid surfaces when the solution was drop-casted on the Si substrate [29]. However, in this study, no fiber structure was discernible, indicating that the film consisted of rapidly formed polycrystallites without sufficient time to grow one-dimensionally on the substrate. Such formation of polycrystallites can yield reciprocal images with numerous diffraction spots if those crystals are perpendicularly aligned to the substrate.

Conversely, the thicknesses of the prepared films were thought to be crucial in determining the degree of alignment, and there was no evidence that the MO β Gal could form perpendicularly aligned to Si(100) substrates, regardless of the film thickness. Since the conventional X-ray beam is not as brilliant when compared to a synchrotron-sourced X-ray beam, the use of greatly aligned crystalline films is a must in order to obtain fine profiles with high resolution using such X-ray sources. From this consideration, the aligning states of crystalline films with different thickness were compared.

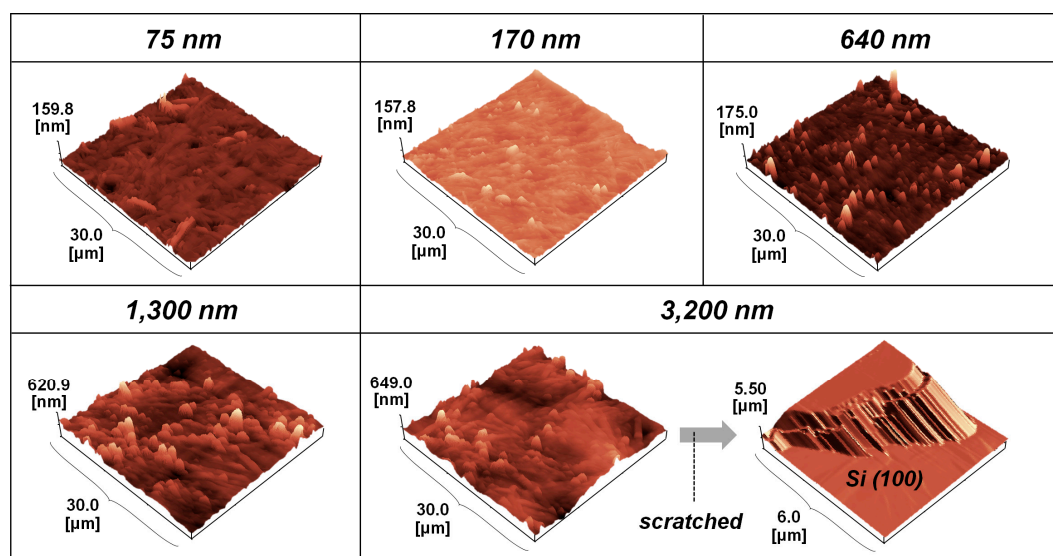


Figure 2. Atomic force microscopy (AFM) images of MO β Gal hemihydrate polycrystalline films with various thicknesses. For the 3200-nm-thick film, the scratched image is also depicted on the right.

Figure 3 shows the results of GIXD analysis for MO β Gal hemihydrate films of 75-, 170-, 640-, 1300-, and 3200-nm-thick films. These data points were obtained with fixed incident angles of 0.15° and 1.4°. Here, the lower angle was less than the critical angle, α_c , and for the material that constituted the radiated film, the phenomenon of total reflection occurs.

For MO β Gal hemihydrate film, electron density, ρ [$e/\text{Å}^3$], was calculated by [(electron density in mole) \times density (g in cm^3) \times molecular weight] as 0.38, where density was used as 1.15 predicted in the previous work (please see the Supporting Information of ref. [24]). Therefore, the α_c of the film was approximately estimated to be 0.163° using the equation $\alpha_c = \lambda \times (r_e \rho / \pi)^{1/2}$ [30], where $r_e \rho$ is the scattering length density and λ is 1.5418 Å (Cu K α radiation). Therefore, in the case where the incident angle is 0.15°, only the surface crystalline region information is obtained. On the other hand, 1.4° is much higher than α_c , and X-ray radiation can penetrate deeply the film to afford sufficient information along the depth direction. Essentially, the peak intensity tends to increase as the film thickness increases.

In Figure 3a, the reflection spots for thin films, such as the 75 nm-thick film, were drastically obscured under these conditions due to the low intensity of diffraction spots, whereas those for thicker films were clearer. However, it was apparent that half of the concentric diffraction rings, as indicated by the white arrows, became clearer for the thicker films, regardless of the incident angles. Such rings, so-called Debye–Scherrer rings, as produced by Bragg reflections, are obtained when an X-ray falls on a mass of tiny crystals in all of the orientations. It means that the crystals in thicker films have a low degree of alignment. In order to obtain quantitative data for comparison, the β -scan profiles for the perpendicularly aligned reciprocal spot at the (200) index were depicted and analyzed by fitting with Gaussian distribution functions. Figure 3b shows a representative result and the integration area. In Figure 3c, the results of ω , which correspond to full width at half maximum (FWHM) for the profiles, were compared as a function of film thickness with the three incident angles: 0.15°, 1.4°, and 2.4°. It was noteworthy that as the film thickness increased from 75 nm, each ω with the various incident angles decreased. Reversely, the increase in film thickness above 640 nm increased it. When considering the factors of the alignment degree and peak intensity, relatively thick films were thought to be adequate for obtaining a GIXD image with a higher resolution. This is because thinner films exacerbate both factors and thicker films exacerbate the high degree of alignment. The confinement effect can somewhat decrease the degree of crystalline alignment for thinner films [31,32], and the rapid crystallization might reduce the alignment degree for the thicker films. Thus, we determined that the use of relatively thick MO β Gal films (thickness = 640 nm) was best for further analysis. However,

unexpectedly, despite the removal of the Debye–Scherer ring influence on the GIXD profile with the 640-nm-thick film and that relatively sufficient intensity was obtained, the diffraction spots in the reciprocal image were unclear, in particular, in the 0.15° incident angle GIXD profile (Figure 3a). However, the diffraction spots at higher diffraction angle regions seemed to be clearer for the GIXD profiles that were obtained with an incident angle of 1.4° .

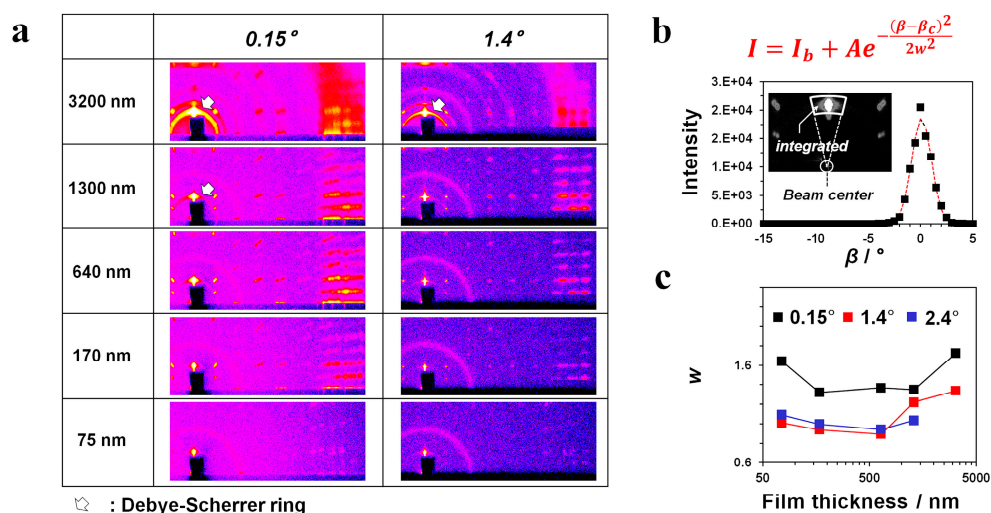


Figure 3. (a) GIXD images obtained for $\text{MO}\beta\text{Gal}$ hemihydrate crystalline films with different thicknesses. Radiation time = 1800 s. Film thicknesses and incident angles are depicted in the figure. (b) Representative β -scan profiles around the (200) reflection and the fitting curve (dotted line) using a Gaussian distribution function. The inset shows the integrated area and I_b is the intensity of baseline, β_c is the centre of azimuth (0°) and A is constant. (c) w , full width at half maximum (FWHM), obtained by fitting the β -scan profiles for the films with different thicknesses and incident angles.

2.2. GIXD Analysis with Different Incident Angles and Radiation Time

As discussed in Section 2.1, the GIXD analysis with an incident angle of 0.15° failed to provide good reciprocal images using the conventional X-ray source (Figure 3a). In addition to the relatively rough surface of the thick films, as observed in the AFM images (Figure 2), and the large beam size of commercial X-ray sources, which is needed for sufficient brilliance, lower incident angle conditions afforded more reciprocal points and should approximately fulfil Ewald's condition, which is often called "reflections under nearly-on-Bragg conditions" by crystallographers. Peak splitting can be caused by additional scattering from the purely substrate-reflected beam and refraction effects occur for the GIXD measurements [33]. Even for profiles that were obtained with synchrotron radiation, the peak splitting for each diffraction spot were somewhat recognizable (Figure 1b). Alternatively, as shown in Figure 3, as the X-ray beam incident angle increases, fewer reciprocal points seemed to approximately fulfil Ewald's condition, allowing for the removal of such two-beam effects. To further confirm the effect of incident angle on the GIXD profiles, the effect of the incident angle on the GIXD profiles was studied more carefully.

Figure 4a shows the results of GIXD analysis for $\text{MO}\beta\text{Gal}$ films, with a film thickness of 640 nm and with different incident angles: 0.1° , 0.15° , 0.2° , 0.4° , 0.8° , 1.2° , 1.4° , 1.6° , 1.8° , 2.0° , 2.2° , and 2.4° . We further compared the one-dimensional profiles to confirm the diffraction spots of $(0kl)$, $(1kl)$, $(2kl)$, and $(3kl)$, respectively (Figure 4b). Those profiles were derived by cutting the equatorial line along the x -axis in the GIXD images. In Figure 4b, the profiles with black lines indicate that no diffraction spots were attained due to their lower diffraction angles in the 2θ direction when compared to the incident angles, while the profiles with red and blue lines were the reflection profiles from the $\text{MO}\beta\text{Gal}$ hemihydrate crystal. Here, the blue lines were obtained with lower incident angles than 0.8° , and the red lines were obtained with higher incident angles than 1.2° . From these profiles, two characteristic tendencies were discernible.

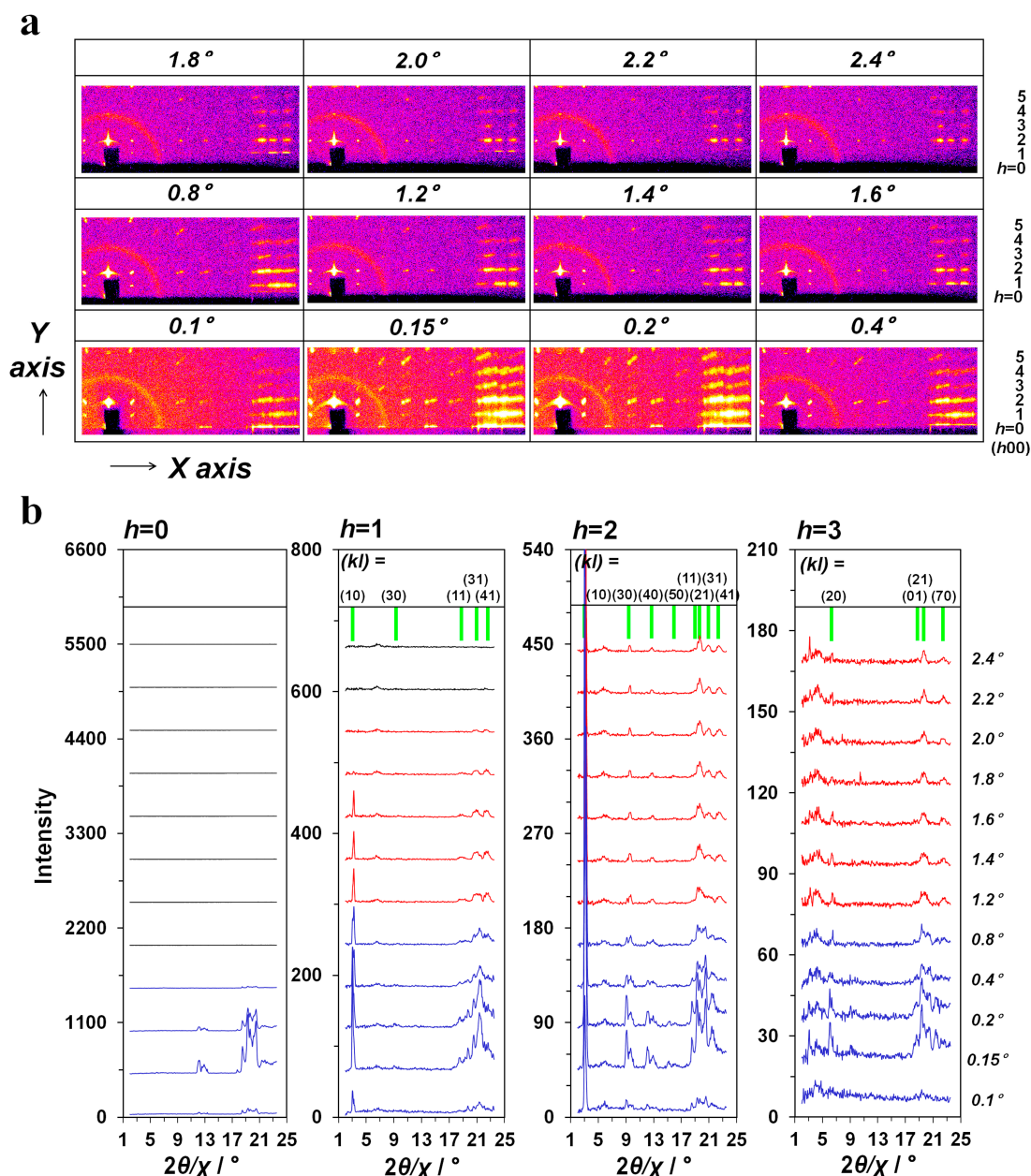


Figure 4. (a) GIXD images obtained for 640-nm-thick MO β Gal hemihydrate crystalline films with different incident angles and a fixed radiation time of 1800 s. (b) One-dimensional profiles derived by cutting the equatorial line from GIXD images at the ($0kl$), ($1kl$), ($2kl$), and ($3kl$) reflection planes, respectively. Black lines indicate that no reflections were observed.

At first, the diffraction spots disappeared at low h index reflections as the incident angle increased. For instance, a series of reflections at ($0kl$) completely disappeared for the GIXD images with incident angles greater than 0.8° . Moreover, even a series of reflection spots at ($1kl$) completely vanished for the GIXD images with incident angles greater than 2.2° . These results arise from the difficulty of capturing reflections from angles that are lower than the corresponding incident angle. This is one of the reasons why an incident angle near the total reflection angle is preferred for GIXD analysis. On the other hand, as the second characteristic of such high-incident angle X-ray sources, some of the diffracted peaks (red lines in Figure 4b) in the reciprocal angles become more clear than those that are obtained with low-incident angle X-rays (blue lines in Figure 4b). That is, multiple and/or connected broad diffraction peaks appeared in the GIXD profiles with the low-incident angles due to

the two-beam effect, which makes the peaks difficult to assign individually. On the other hand, under the high-incident angle conditions, the number of reflection points at which the Ewald sphere condition is fulfilled, and peak splitting decreases and only fine spots remained, which become individually separated enough to be assigned. From these results, it was found that the use of a high-incident angle was effective for identifying the reflection spots at higher angles along the perpendicular direction than from the corresponding incident angle.

We also investigated the peak resolution factor. The two-dimensional X-ray detector, Pilatus 100 K (Rigaku Corp.), which was used in the measurements with the NANO-Viewer apparatus (Rigaku Corp.), is based on pixelated photon-counting technology, and the peak intensity can be increased without noise contamination, even with sustained radiation. In other words, the degree of resolution can increase with the radiation time. With synchrotron radiation, the highly brilliant reciprocal image could be attainable with short radiation times of less than 5 s (Figure 1). But, in the laboratory scale case with the NANO-Viewer system (Rigaku Corp.), because of the lower X-ray flux of the conventional system, several ambiguities for peak assignment existed, even with a measurement time of 1800 s (Figure 4). The $\text{MO}\beta\text{Gal}$ hemihydrate crystal was highly stable under the conventional X-ray radiation conditions and sustained measurements over a longer timescale were applicable.

In Figure 5a, the results of GIXD analysis that were obtained for the 640-nm-thick $\text{MO}\beta\text{Gal}$ films with incident angles of 1.4° and 2.4° , and with different radiation times from 600 to 7200 s, are depicted. The one-dimensional profiles, to confirm the diffraction peaks of $(2kl)$ and $(5kl)$, are shown in Figure 5b. For the diffraction peaks of the $(2kl)$ series, even a short measurement time, such as 600 s, could allow us to assign the indexes of those peaks; however, it was difficult for the $(5kl)$ series peaks. After radiation for 3600 s, the diffraction profile became well resolved, with the incident angle of 2.4° , indicating the importance of the longer radiation times. In addition, the diffraction peaks around 20° did not become well separated for the 1.4° incident angle results, suggesting that the resolution ability with the higher incident angle was better than with the lower incident angle for diffraction peaks at higher h indexes. This is despite the fact that the incident angles were much higher than the total reflection angle. However, at this stage, several ambiguities for peak assignment still remained for the $(0kl)$ and $(1kl)$ series.

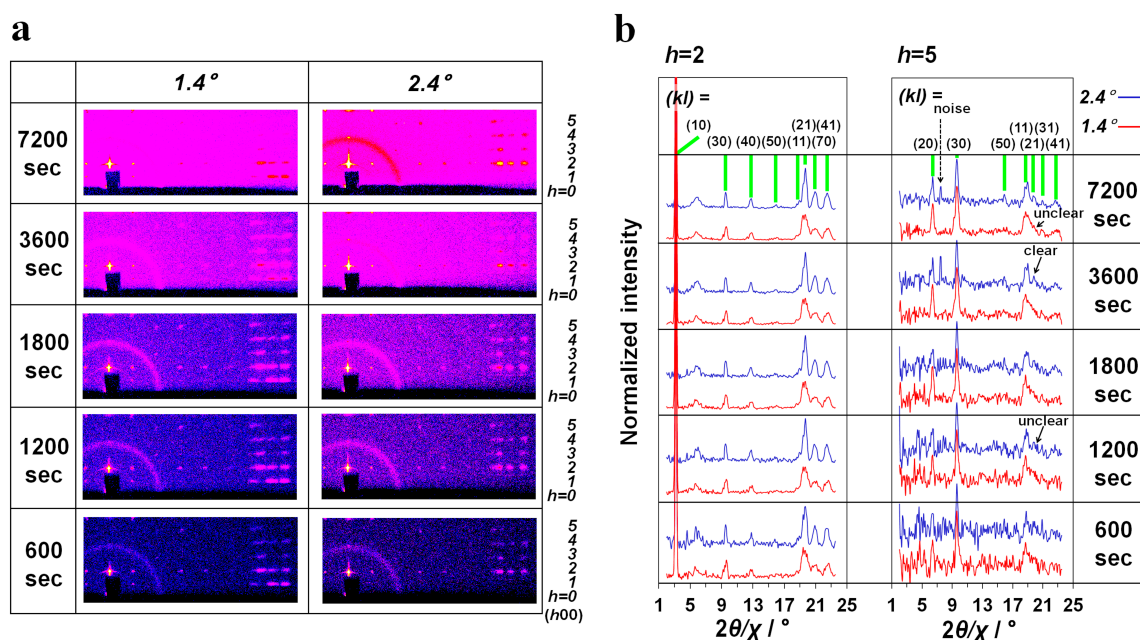


Figure 5. (a) GIXD images obtained for 640-nm-thick $\text{MO}\beta\text{Gal}$ hemihydrate crystalline films with incident angles of 1.4° and 2.4° and different radiation times. (b) One-dimensional profiles corresponding to the $(2kl)$ and $(5kl)$ reflection planes derived by cutting the equatorial line in the GIXD image.

2.3. Out-of-Plane and In-Plane Measurement

SmartLab (Rigaku Corp.) equips parallel beam optics with a multilayer mirror and parallel collimator. One of the parallel beam characteristics is to reduce the peak shift and the broadness that is derived from positional deviations in the samples. The higher resolution for $(0kl)$ and $(1kl)$ series reflections was thought to be attainable using in-plane measurements with a parallel beam. We applied in-plane analysis to assign the diffraction peaks that seemed difficult to identify using GIXD analysis, as demonstrated in Sections 2.1 and 2.2.

As a preliminary measurement, the out-of-plane measurement ($2\theta/\omega$ scan) was carried out to confirm the diffraction angles with the specular-reflections for the $\text{MO}\beta\text{Gal}$ film (Figure 6a). In the one-dimensional X-ray diffraction profile that was obtained using the $2\theta/\omega$ scan, several diffraction peaks, assigned as $(h00)$ reflections, where h is an even number, were observed. Diffraction peaks obtained using a 2θ scan with a fixed incident angle of 0.15° only afforded the (200) reflection, owing to the low reflection intensity arising from the non-specular conditions. As shown in Figure 6b, obtained from GIXD analysis using the NANO-Viewer system (Rigaku Corp.), despite the reduction in reflected area as the incident angle increased, the peak intensity at the (200) index increased up to approximately 1.80° , where specular-reflection occurred. The peak intensity at (200) decreased due to the loss of specular reflection when the incident angle became higher, whereas another peak intensity, assigned as the (400) reflection, grew, which was due to approaching the incident angle (7.14°), at which point specular-reflection occurs for the (400) reflection.

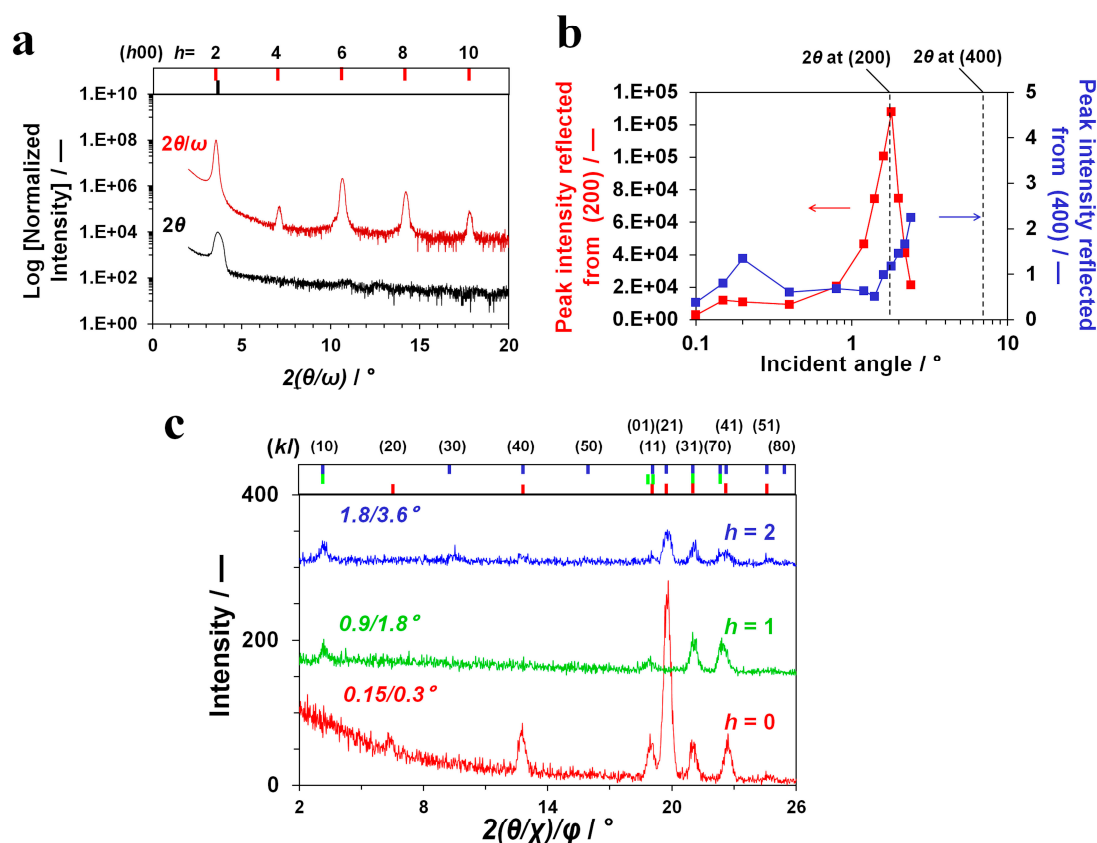


Figure 6. X-ray analyses of 640-nm-thick $\text{MO}\beta\text{Gal}$ hemihydrate crystalline films. (a) Out-of-plane profiles. Comparison of profiles obtained with $2\theta/\omega$ and 2θ scans using an incident angle of 0.15° . (b) Peak intensities at the (200) and (400) reflections vs. incident angles. (c) In-plane profiles. The angles of (incident/detected) in the 2θ range are noted inside the figure.

In-plane measurements were next performed. The location of the detector was set to detect the $(0kl)$, $(1kl)$, and $(2kl)$ reflections, based on the $2\theta/\omega$ profile and GIXD image. Figure 6c shows the results of the $2(\theta/\chi)/\phi$ scan for the 640-nm-thick $\text{MO}\beta\text{Gal}$ hemihydrate crystalline films. Clear diffraction peaks, even at higher diffraction angles, were confirmed for a series of one-dimensional profiles from the $(0kl)$ to $(2kl)$ planes. On the other hand, the results at higher h values than four afforded poor profiles due to the low X-ray energy source (data not shown). For the parallel plane to $(0kl)$, at least six diffraction spots were confirmed between 18.94° and 22.72° . The profiles that were obtained for the parallel planes of $(1kl)$ and $(2kl)$ were also well assigned, as depicted in the top of the Figure 6c.

2.4. Global Reciprocal Image of $\text{MO}\beta\text{Gal}$ Hemihydrate Prepared by Combining Data of Two-Dimensional GIXD Analysis with In-Plane Measurements

Figure 7 shows a reciprocal image with many reciprocal spots obtained from the two-dimensional GIXD analysis and in-plane measurements, which are also summarized in Table 1. In Figure 7, the reciprocal spots that were further observed by synchrotron radiation were also denoted by red circles. Several additional reflection spots were apparently identified using via the synchrotron radiation source. In addition, the raw reciprocal image from the synchrotron radiation covered the high h index (Figure 1b). For instance, only two reflections corresponding to the $(h0l)$ indexes, i.e., (101) and (301) were detected using a commercial radiation source, whereas the result of the reciprocal image that was obtained via the synchrotron radiation with a large detector further detected (501) , (701) , (901) , and $(10\ 01)$. However, the data, even without such reciprocal spots obtained with synchrotron radiation, could resolve the characteristic reciprocal spots of (200) , (110) , and (011) , which could not be assigned by conventional PXRD analysis, as shown in Figure 1c. In addition, the lattice parameters a , b , and c were successfully determined; at least, the limiting conditions that $(h00)$ and $(0k0)$ are even were identified (Table 1). Reflections corresponding to $(00l)$ were not observed. In addition, it was difficult to observe the (002) reflection because of the low intensity of the in-plane profile (data not shown). However, at least reflections corresponding to (001) must be detected on account of the extinction law. In addition, although the information of $h + l$ for $(h0l)$ was not sufficient for identification, limitations were not observed in terms of $h + k$ and $k + l$ for $(hk0)$ and $(0kl)$. Summarizing these conditions, an appropriate space group is not available for which an additional extinction law such as $h + l = \text{even}$ for $(h0l)$; hence, $P2_12_12_1$ in an orthorhombic system is reasonable for selection. Thus, it is reasonable to conclude that the global reciprocal image of the $\text{MO}\beta\text{Gal}$ hemihydrate is sufficiently constructed by the combination of the results that were obtained from the GIXD analysis with a two-dimensional detector and in-plane measurements using a point detector. In particular, the determination of lattice parameters can demonstrate the uniqueness of the crystal structure of $\text{MO}\beta\text{Gal}$ hemihydrate.

Unfortunately, assigning the molecular crystal packing for the $\text{MO}\beta\text{Gal}$ hemihydrate crystal appeared to be difficult without the aid of high quality computer simulations. Moreover, accurate computer simulation operations would not be trivial because of the large Z value, more than 10 for the crystal [24], and the intrinsic nature of sugar moieties, where a variety of intramolecular or intermolecular hydrogen bonding interactions can exist with several conformational geometries [34]. However, we believed that even if accurate molecular packing could not be determined, unveiling the unique crystal structure, which did not appear to be a simple bilayer structure (as reported thus far for synthetic glycolipid compounds [2–10]), but to be a modulated structure [24], must be an important factor when determining the unknown characteristics of synthetic glycolipids. This is because the synthetic glycolipids have been expected to serve as relevant model systems for the complex structural transitions that can occur in the normal functions of cell membrane glycolipids.

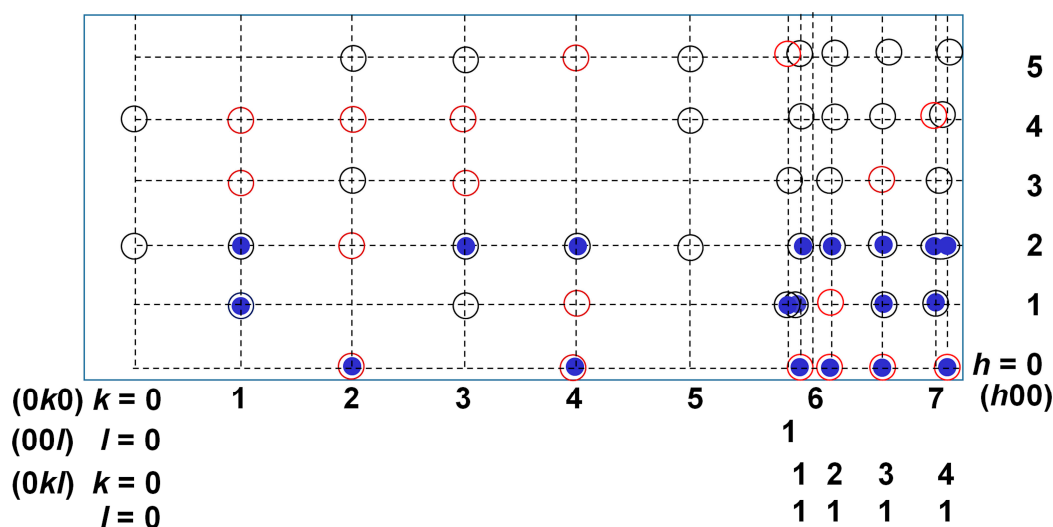


Figure 7. Illustrated reciprocal image prepared by combining the data of the GI-XD images (open black circle; Figure 5a) and the in-plane profiles (filled blue circle; Figure 6c). Open red circles indicate the reflection spots determined based on the result obtained with the GIXD image with synchrotron radiation (Figure 1b).

Table 1. The (hkl) reflections measured using commercial X-ray sources in this study.

h	k	l	h	k	l	h	k	l
0	1	1	2	1	0	4	0	0
0	2	1	2	3	0	4	1	1
0	2	0	2	4	0	4	2	1
0	3	1	2	5	0	4	3	1
0	4	0	2	1	1	4	4	1
0	4	1	2	2	1	4	5	0
1	1	0	2	3	1	5	1	1
1	0	1	2	4	1	5	2	0
1	1	1	2	7	0	5	2	1
1	3	0	3	0	1	5	3	0
1	3	1	3	2	0	5	3	1
1	7	0	3	2	1	5	4	1
2	0	0	3	7	1	5	5	0

For $(h00)$, $(0k0)$ and $(00l)$ reflections, reflections corresponding to odd values for h , k , and l were not detected; the following lattice constants were obtained; $a = 49.5 \text{ \AA}$, $b = 27.7 \text{ \AA}$ and $c = 4.74 \text{ \AA}$. In addition, the $P2_12_12_1$ space group in the orthorhombic crystal system was strongly suggested.

3. Materials and Methods

MO β Gal was purchased from Santa Cruz Biotechnology, Inc. (Santa Cruz, CA, USA) and used as received. Film samples were prepared by spin coating hot aqueous MO β Gal solutions on $2 \times 2 \text{ cm}^2$ Si(100) substrates (Electronics and Materials Corp., Hyogo, Japan) at 4000 rpm for 50 s. Subsequent annealing at room temperature in a sealed container resulted in the hemihydrate crystalline films. The thickness of each film was determined using the method that we previously reported on [24]. GIXD measurements with a synchrotron radiation source were performed at BL03XU, SPring-8 (Hyogo, Japan). The diffraction patterns were obtained using an image-plate detector system (R-AXIS IV, Rigaku Corp.) with an incident angle of 0.17° (wavelength = 0.100 nm) for 3 s. Atomic force microscopy (AFM; SPM-9600, Shimadzu Co.) was used for the observation of hemihydrate crystalline film morphology. XD analyses with conventional X-ray sources were performed as follows: First, two-dimensional GIXD measurements under an ambient atmosphere were performed with various incident angles between 0.10° to 2.4° using the NANO-Viewer (Rigaku Corp.) (40 kV, 30 mA), where the XD pattern was

detected using a two-dimensional detector, Pilatus 100K (Rigaku Corp.), and Cu K α (0.15418 nm) was used as the X-ray beam. XD measurements with in-plane and out-of-plane configurations to detect the crystalline structure perpendicular and parallel to the substrate directions, respectively, were performed using a SmartLab (Rigaku Corp.) (40 kV, 30 mA), with a one-dimensional D/teX Ultra 2 (Rigaku Corp.) detector. Cu K α (0.15418 nm) was used as the X-ray beam.

4. Conclusions

We analyzed perpendicularly aligned MO β Gal polycrystalline films using laboratory-scale X-ray apparatuses, NANO-Viewer (Rigaku Corp.), and SmartLab (Rigaku Corp.), and compared the results to those obtained with synchrotron radiation. The structural resolution was limited when compared to the structural data obtained with a synchrotron-sourced X-ray beam. In particular, the GIXD analysis using a low-incident angle, near the total reflection angle, showed that peak splitting and the diffraction spots were unclear, while such peak splitting was also observed in the GIXD profile obtained using a synchrotron radiation source. In order to obtain better resolution, we used much higher incident angles than the total reflection angles, longer radiation times and appropriate film thickness with high alignment; the clarity of the reciprocal profiles increased with the increase in the incident angle. These advantages afforded highly resolved reciprocal spots. Here, the reflection data at lower angle regions below the corresponding incident angles disappeared due to the lack of diffraction spots below the incident angle in the GIXD image. However, the use of PXRD analysis with in-plane and out-of-plane configurations successfully complemented those lost reciprocal spots for the reciprocal image that was obtained with high-incident angles. By combining the data obtained from analyses of XD and PXRD, we successfully obtained excellent reciprocal images of the MO β Gal hemihydrate crystalline films, which allowed for us to determine the lattice parameters and crystal symmetry without using a synchrotron radiation source. To determine the space group, $P2_12_12_1$ was strongly suggested on the basis of the data obtained herein, whereas the use of the synchrotron radiation source permits the analysis of such crystal structural parameter in more detail.

The developed method for using a laboratory-scale diffractometer must contribute to the investigations on both the static and dynamic structural aspects of synthetic glycolipid crystallites, which are still not completely clarified. If the apparatus settings, such as X-ray flux, energy, degree of coherency, and detector type, were different, then other combinations or non-cooperating methodologies may be applicable other than the experimental setting that is utilized here.

Acknowledgments: We thank Yukihiro Ozaki (Department of Chemistry, Kwansei Gakuin University, Japan) for help with the FTIR measurements. This study was supported in part by the Japan Society for the Promotion of Science (Grant-in-Aid for Scientific Research (C) 17KO5617) and the MEXT-Supported Program for the Strategic Research Foundation at Private Universities (S1201027), 2012–2016. The synchrotron radiation experiments were performed in the first hutch of BL03XU, SPring-8 (Hyogo, Japan), as constructed by the Consortium of Advanced Soft material BeamLine (FSBL) with the approval of JASRI (Proposal no. 2015B7254).

Author Contributions: S.O. and I.T. conceived, designed and performed the experiments, analyzed the data and wrote the paper.

Conflicts of Interest: The authors declare no conflict of interest.

References

1. Fischer, E. Ueber die glucoside der alkohole. *Ber. Dtsch. Chem. Ges.* **1893**, *26*, 2400–2412. [[CrossRef](#)]
2. Pascher, I.; Sundell, S. Molecular arrangements in sphingolipids. The crystal structure of cerebroside. *Chem. Phys. Lipids* **1977**, *20*, 175–191. [[CrossRef](#)]
3. Abrahamsson, S.; Dahlén, B.; Pascher, I. Molecular arrangements in glycosphingolipids: The crystal structure of glucosylphytosphingosine hydrochloride. *Acta Cryst. B* **1977**, *B33*, 2008–2013. [[CrossRef](#)]
4. Jeffrey, G.A. Carbohydrate liquid crystals. *Acc. Chem. Res.* **1986**, *19*, 168–173. [[CrossRef](#)]
5. Abe, Y.; Harata, K. Crystal structures of glycolipids. In *Polysaccharides Structural Diversity and Functional Versatility*, 2nd ed.; Dumitriu, S., Ed.; CRC Press: Boca Raton, FL, USA, 2004; pp. 743–771.
6. Jeffrey, G.A. Carbohydrate liquid crystals. *Mol. Cryst. Liq. Cryst.* **1984**, *110*, 221–237. [[CrossRef](#)]

7. Jeffrey, G.A.; Wingert, L.M. Carbohydrate liquid crystals. *Liq. Cryst.* **1992**, *12*, 179–202. [[CrossRef](#)]
8. Moews, P.C.; Knox, J.R. The crystal structure of 1-decyl α -D-glucopyranoside: A polar bilayer with a hydrocarbon subcell. *J. Am. Chem. Soc.* **1976**, *13*, 6628–6633. [[CrossRef](#)]
9. Jeffrey, G.A.; Yeon, Y. The crystal structure of a 1:1 complex of *n*-octyl α - and β -D-glucopyranoside at 123K. *Carbohydr. Res.* **1992**, *237*, 45–55. [[CrossRef](#)]
10. Adasch, V.; Hoffmann, B.; Milius, W.; Platz, G.; Voss, G. Preparation of alkyl α - and β -D-glucopyranosides, thermotropic properties and X-ray analysis. *Carbohydr. Res.* **1998**, *314*, 177–187. [[CrossRef](#)]
11. Zhang, W.; Oliver, A.G.; Vu, H.M.; Duman, J.G.; Serianni, A.S. Methyl 4-O- β -D-xylopyranosyl β -D-mannopyranoside, a core disaccharide of an antifreeze glycolipid. *Acta Cryst. C* **2013**, *C69*, 1047–1050. [[CrossRef](#)] [[PubMed](#)]
12. Dorset, D.L.; Rosenbusch, J.P. Solid state properties of anomeric 1-O-*n*-octyl-D-glucopyranosides. *Chem. Phys. Lipids* **1981**, *29*, 299–307. [[CrossRef](#)]
13. Jeffrey, G.A.; Bhattacharjee, S. Carbohydrate liquid-crystals. *Carbohydr. Res.* **1983**, *115*, 53–58. [[CrossRef](#)]
14. Pfannemuller, B.; Welte, W.; Chin, E.; Goodby, J.W. Liquid-crystalline behaviour in the *n*-alkyl gluconamides and other related carbohydrates. *Liq. Cryst.* **1986**, *1*, 357–370. [[CrossRef](#)]
15. Häntzschel, D.; Schulte, J.; Enders, S.; Quitzsch, K. Thermotropic and lyotropic properties of *n*-alkyl- β -D-glucopyranoside surfactants. *Phys. Chem. Chem. Phys.* **1999**, *1*, 895–904. [[CrossRef](#)]
16. Ma, Y.-D.; Takada, A.; Sugiura, M.; Fukuda, T.; Miyamoto, T.; Watanabe, J. Thermotropic liquid crystals based on oligosaccharides. *n*-Alkyl 1-O- β -D-cellobioside. *Bull. Chem. Soc. Jpn.* **1994**, *67*, 346–351. [[CrossRef](#)]
17. Dumoulin, F.; Lafont, D.; Boullanger, P.; Mackenzie, G.; Mehl, G.H.; Goodby, J.W. Self-organizing properties of natural and related synthetic glycolipids. *J. Am. Chem. Soc.* **2002**, *124*, 13737–13748. [[CrossRef](#)] [[PubMed](#)]
18. Ericsson, C.A.; Ericsson, L.C.; Kocherbitov, V.; Söderman, O.; Ulvenlund, S. Thermotropic phase behaviour of long-chain alkylmaltosides. *Phys. Chem. Chem. Phys.* **2005**, *7*, 2970–2977. [[CrossRef](#)] [[PubMed](#)]
19. Jeffrey, G.A.; Maluszynska, H. The crystal structure and thermotropic liquid-crystal properties of *N*-*n*-undecyl-D-glucoamide. *Carbohydr. Res.* **1990**, *207*, 211–219. [[CrossRef](#)]
20. Kocherbitov, V.; Söderman, O. Phase diagram and physicochemical properties of the *n*-octyl α -D-glucoside/water system. *Phys. Chem. Chem. Phys.* **2003**, *5*, 5262–5270. [[CrossRef](#)]
21. Ericsson, C.A.; Ericsson, L.C.; Ulvenlund, S. Solid-state phase behavior of dodecylglycosides. *Carbohydr. Res.* **2005**, *340*, 1529–1537. [[CrossRef](#)] [[PubMed](#)]
22. Ogawa, S.; Asakura, K.; Osanai, S. Thermotropic and glass transition behaviors of *n*-alkyl β -D-glucosides. *RSC Adv.* **2013**, *3*, 21439–21446. [[CrossRef](#)]
23. Rivnay, J.; Mannsfeld, S.C.B.; Miller, C.E.; Salleo, A.; Toney, M.F. Quantitative determination of organic semiconductor microstructure from the molecular to device scale. *Chem. Rev.* **2012**, *112*, 5488–5519. [[CrossRef](#)] [[PubMed](#)]
24. Ogawa, S.; Ozaki, Y.; Takahashi, I. Structural insights into solid-to-solid phase transition and modulated crystal formation in octyl- β -D-galactoside crystals. *ChemPhysChem* **2016**, *17*, 2808–2812. [[CrossRef](#)] [[PubMed](#)]
25. Goodby, J.W. Liquid crystal phases exhibited by some monosaccharides. *Mol. Cryst. Liq. Cryst.* **1984**, *110*, 205–219. [[CrossRef](#)]
26. Yamamoto, A.; Abuillan, W.; Burk, A.S.; Körner, A.; Ries, A.; Werz, D.B.; Demé, B.; Tanaka, M. Influence of length and conformation of saccharide head groups on the mechanics of glycolipid membranes: Unraveled by off-specular neutron scattering. *J. Chem. Phys.* **2015**, *142*, 154907. [[CrossRef](#)] [[PubMed](#)]
27. Masunaga, H.; Ogawa, H.; Takano, T.; Sasaki, S.; Goto, S.; Tanaka, T.; Seike, T.; Takahashi, S.; Takeshita, K.; Nariyama, N.; et al. Multipurpose soft-material SAXS/WAXS/GISAXS beamline at SPring-8. *Polym. J.* **2011**, *43*, 471–477. [[CrossRef](#)]
28. Ogawa, H.; Masunaga, H.; Sasaki, S.; Goto, S.; Tanaka, T.; Seike, T.; Takahashi, S.; Takeshita, K.; Nariyama, N.; Ohashi, H.; et al. Experimental station for multiscale surface structural analyses of soft-material films at SPring-8 via a GISAXS/GIXD/XR-integrated system. *Polym. J.* **2013**, *45*, 109–116. [[CrossRef](#)]
29. Ogawa, S.; Koga, M.; Asakura, K.; Takahashi, I.; Osanai, S. Coagel Prepared from Aqueous Octyl β -D-Galactoside Solution. *J. Surfact. Deterg.* **2017**, *20*, 255–261. [[CrossRef](#)]
30. Tolan, M. Springer Tracts in Modern Physics. In *X-ray Scattering from Soft-Matter Thin Films. Materials Science and Basic Research*; Springer: Berlin, Germany, 1999; ISBN 978-3-662-14218-9.

31. Reddy, K.R.; Ogawa, S.; Sato, H.; Takahashi, I.; Ozaki, Y. Evolution of intermediate and highly ordered crystalline states under spatial confinement in poly(3-hydroxybutyrate) ultrathin films. *Macromolecules* **2016**, *49*, 4202–4210. [[CrossRef](#)]
32. Yoshida, H.; Inaba, K.; Sato, N. X-ray diffraction reciprocal space mapping study of the thin film phase of pentacene. *Appl. Phys. Lett.* **2007**, *90*, 181930. [[CrossRef](#)]
33. Breiby, D.W.; Bunk, O.; Andreasen, J.W.; Lemke, H.T.; Nielsen, M.M. Simulating X-ray diffraction of textured films. *J. Appl. Cryst.* **2008**, *41*, 262–271. [[CrossRef](#)]
34. Ahmadi, S.; ManickamAchari, V.; Hussain, Z.; Hashim, R. Epimeric and anomeric relationship of octyl- α -D-glucoside/galactosides: Insight from density functional theory and atom in molecules studies. *Comput. Theor. Chem.* **2017**, *1108*, 93–102. [[CrossRef](#)]



© 2017 by the authors. Licensee MDPI, Basel, Switzerland. This article is an open access article distributed under the terms and conditions of the Creative Commons Attribution (CC BY) license (<http://creativecommons.org/licenses/by/4.0/>).